The Meteoritical Society

Meteoritics & Planetary Science 46, Nr 2, 199–217 (2011)
doi: 10.1111/j.1945-5100.2010.01145.x

Pd and Ag metal-silicate partitioning applied to Earth differentiation and core-mantle exchange

Kevin T. WHEELER[1†], David WALKER[1*], and William F. McDONOUGH[2]

[1]Lamont Doherty Earth Observatory and Department of Earth and Environmental Sciences, Columbia University, Palisades, New York 10964, USA
[†]Present address: 20 Sellers Ave, Lexington, Virginia 24450, USA
[2]Department of Geology, University of Maryland, College Park, Maryland 20742, USA
[*]Corresponding author. E-mail: dwalker@ldeo.columbia.edu

(Received 21 September 2007; revision accepted 11 October 2010)

Abstract–Pd and Ag partitioning between liquid Fe metallic sulfide and liquid silicate under plausible magma ocean conditions constrains potential core ^{107}Ag content and the origin of observed Pd and Ag mantle abundances. $D_{Pd}^{metallic\ sulfide/silicate}$ (element concentration in metallic liquid/concentration in silicate liquid) in our experiments is insensitive to S content and temperature, but increases with total Pd content. $D_{Pd}^{metallic\ sulfide/silicate}$ at low Pd concentration ranges from approximately 150–650. Metallic sulfide Pd content and silicate Pd content anticorrelate in our study. A curved silicate saturation surface in the Fe sulfide–silicate Pd ternary can explain both the metallic sulfide–silicate Pd anticorrelation and interstudy differences in $D_{Pd}^{metallic\ sulfide/silicate}$ behavior. The size and shape of the curved silicate phase volume may respond to physical and chemical conditions, reducing the general applicability of D calculations. Ag becomes decreasingly siderophile as S increases: $D_{Ag}^{metallic\ sulfide/silicate}$ decreases from 144 at 0 wt% S to 2.5 at 28 wt% S added to the starting metal sulfide liquid. Model calculations indicate that 1% core material incorporated into the Hawai'ian plume would yield a ^{107}Ag signature on the surface smaller than detectable by current analytical techniques. Observed Pd and Ag mantle depletions relative to bulk Earth are consistent with depletions calculated with the data from this study for a magma ocean scenario without additional accretionary input after core formation.

INTRODUCTION

The extent to which the metal and silicate portions of early Earth achieved chemical equilibrium is partially reflected today in the chemical compositions of the core, mantle and crust. Can the observed composition of Earth's mantle be approximated by metal/silicate equilibrium, or are additional processes of accretion and differentiation required? Constraint on the extent of equilibration between the core and bulk silicate Earth (mantle and crust) through experiment is the goal of this study.

Core-Mantle Interaction and Timing of Differentiation

The timing of core formation, the extent of differentiation, and the existence of subsequent core-mantle interaction can be addressed with fractionated parent–daughter isotopic systems. Parent–daughter isotopic pairs with different siderophile behaviors are susceptible to fractionation during core formation and inner–outer core differentiation. If core formation and differentiation occurred within the lifetime of the radioactive parent, potentially observable radiogenic daughter excess would develop in the parent-concentrating phase.

The ^{107}Pd-^{107}Ag parent–daughter isotopic decay system is a candidate for use in both constraining the timing of early planetary fractionation events and for determining whether Earth's core material is incorporated into mantle plumes. ^{107}Pd decays to ^{107}Ag with a half-life of 6.5 million years. This relatively short half-life renders the system sensitive to fractionation events occurring within the first 40 million years of

solar system history (i.e., Kelly and Wasserburg 1978). Furthermore, because Pd is more siderophile than Ag (e.g., Jones and Drake 1986; Peach et al. 1990; Fleet et al. 1996) planetary differentiation should result in an enrichment of Pd relative to Ag in planetary cores. If this happened during the lifetime of ^{107}Pd, a correspondingly high ^{107}Ag core signature would develop. If Earth's differentiation occurred within 40 million years (approximately 5 ^{107}Pd half lives) of the beginning of the solar system, an isotopic excess of ^{107}Ag should exist within the core.

Core formation and fractionation events did occur early in the protoplanetary bodies of the solar system, as evidenced by isotopic signatures in iron meteorites. Meteorites provide proxy insights into the possible ^{107}Ag signature of Earth's core. Excess ^{107}Ag (^{107}Ag*) has been observed in many iron and stony iron meteorites, consistent with core formation during the lifetime of ^{107}Pd, leaving open the possibility of a similar signature in Earth's core (e.g., Chen and Wasserburg 1996; Carlson and Hauri 2001). Observed ^{107}Ag* values range from ε^{107}Ag of approximately −15 in meteorite iron sulfide phases to more than ε^{107}Ag of 200 in meteorite iron metal phases relative to terrestrial standard NIST SRM 978a. ^{107}Ag* varies as a function of age and of Pd/Ag concentration. In meteorites, ^{107}Ag abundance commonly correlates positively with Pd/Ag suggesting that excess ^{107}Ag is the result of ^{107}Pd decay, not a nebular condensation effect, and that elemental fractionation happened within the lifetime of ^{107}Pd (Chen and Wasserburg 1996).

A potential place on Earth's surface to detect a ^{107}Ag signal in the core would be the Hawai'ian volcanic rocks. The Hawai'ian hot spot may be the surface manifestation of a mantle plume with deep origins that may have entrained core material (e.g., Ribe and Christensen 1999; Van Keken et al. 2002). If this hypothesized plume incorporated core material before its rise to the surface, the associated lavas may contain a core-like ^{107}Ag signature. Tantalizingly, Walker et al. (1995) directed the search for, and Brandon et al. (1998) reported radiogenic ^{186}Os derived from long-lived ^{190}Pt in Mauna Loa lavas, with one possible explanation being the presence of an outer core component higher in Pt/Os than chondrites. Several workers have analyzed the same lavas for ^{107}Ag and their results remain inconclusive. Hauri et al. (2000) reported elevated ^{107}Ag in Mauna Loa lavas (ε^{107}Ag of 1.5; where 1ε = 1 part in 10,000 ^{107}Ag/^{109}Ag). However, the reported signal is only slightly larger than analytical uncertainty for Ag isotopes (ε^{107}Ag of ±1.3 from Carlson and Hauri 2001). Further analysis by Schonbachler et al. (2007, 2008) have since reduced analytical uncertainty in Ag isotope measurements to ε^{107}Ag of ±0.5, but we are not aware of new measurements on lavas with potential plume components.

An unresolved question, critical to these analyses, is how big would the ^{107}Ag signal be from lavas associated with a plume containing core material? Would the ^{107}Ag signal be larger than current analytical error? The answer depends on three factors (1) timing of metal-silicate fractionation, either in Earth or in Earth-forming protoplanetary bodies, (2) Pd/Ag in Earth, and (3) partitioning of Ag and Pd during metal-silicate fractionation.

Pd/Ag in Planetary Bodies

Pd/Ag varies widely in iron meteorites from approximately 80 in Canyon Diablo to more than 10^5 in many IVA and IVB iron meteorites. This extreme variability is not the outcome of classic planetary differentiation, but is likely the result of differences in volatile element incorporation during the condensation phase of the solar nebula (e.g., Chen and Wasserburg 1996). This large variability of Pd/Ag in iron meteorites makes determining a definitive Earth Pd/Ag ratio and calculating a core ^{107}Ag* difficult. Based on CI carbonaceous chondrite composition (Pd/Ag approximately 2.8; Palme and Jones 2003) and terrestrial volatile depletion trends, McDonough (2003) calculates a bulk Earth Pd/Ag of 20. However, based on mantle ^{107}Ag/^{109}Ag, Carlson and Hauri (2001) suggest that Earth's Pd/Ag could be as high as 88.

Previous Experimental Studies of Ag and Pd Partitioning

Pd and Ag partitioning between solid metal/liquid sulfide and liquid metallic sulfide/liquid silicate systems has been studied previously by experiment, as summarized by Wheeler (2007) and below. Variation of measured experimental $D_{Pd}^{\text{metallic sulfide/silicate}}$ spans several orders of magnitude from approximately 10^3 to 10^7. The range of solid sulfide/silicate D computed from mineral assemblages ranges from approximately 10^3 to $>10^5$. Direct applicability of any of these natural-system studies to a magma ocean metal-silicate fractionation process is uncertain due to vastly different physical conditions and even processes of concentration.

The primary cause for such disparate Pd D-value behavior is poorly established, though not for lack of experimental effort. Experimental fO_2, T, P, sulfide S content, Ni content, and platinum group element (PGE) content have all been explored as influences on Pd partitioning behavior and therefore as sources for interlaboratory disagreement. To this list might be added C content. However, none of these variables has emerged as the major driver. The publications of Fleet,

Crockett, Stone, and their coworkers repeatedly assert that PGEs display non-Henrian behavior resulting in larger metallic sulfide/silicate D with increased experimental PGE concentrations (e.g., Fleet et al. 1991). This behavior has not been reported by other groups until the present study. Oxygen fugacity (fO_2) has gained wider acceptance as an important influence on Pd partitioning. Fleet et al. (1991), Bezmen et al. (1994), Borisov et al. (1994), and O'Neill et al. (1995) all found a negative dependence between Pd's metal sulfide/silicate D and fO_2. However, the magnitude of the fO_2 effect has not been agreed upon. Furthermore, Peach et al. (1994) reported no effect of fO_2/fS_2 on Pd partitioning behavior. Increasing the experimental Ni contents appears to stabilize an otherwise variable Pd D-value but does not appear to influence overall partitioning behavior (e.g., Crocket et al. 1997). Experimental S content has also been reported to have an effect, though the direction and magnitude of that effect is not agreed upon. Fleet et al. (1999) claim that $D_{Pd}^{\text{metallic sulfide/silicate}}$ increases with increasing S content in the sulfide from metal-rich to S-rich compositions. In contrast, the data from other studies suggest the opposite (e.g., Peach et al. 1994). Pressure's influence on Pd partitioning has been tested sparingly. Holzheid et al. (2000) did not identify it as a significant influence on Pd solubility in silicate melts. Righter et al. (2006, 2008), however, observed a strong decrease in D Pd as pressures increase from 1.5 GPa to 15 GPa. Increasing temperature has been documented in several S-free studies to decrease D Pd significantly (e.g., Borisov et al. 1994; O'Neill et al. 1995; and Holzheid et al. 2000). Righter et al. (2006, 2008) observed a similar trend when using MgO capsules and attribute the effect to increasing depolymerization of the silicate melt. Experiments with graphite capsules, however, exhibited no temperature effect on D Pd.

The only partitioning data for Ag of which we are aware is from the study of Jones and Drake (1986). They report a single $D_{Ag}^{\text{metallic sulfide/silicate}}$ of approximately 100 at atmospheric pressure, approximately 1250 °C and 23–27 wt% S in the metal.

Precis

Core formation events in meteorite parent bodies occurred quickly enough for a $^{107}Ag^*$ signature to develop in segregated metallic material. By extension, the same could be true for Earth. Terrestrial Pd/Ag estimates range from 20 to close to 90. Experimental and natural sample partitioning data for Pd between liquid metal and liquid silicate exhibit a wide variation that includes the observed depletions in the mantle as a natural outcome. This study endeavors to constrain better the expected $^{107}Ag^*$ core composition by conducting a series of Pd and Ag partitioning experiments at physical and chemical conditions relevant to core formation in a magma ocean scenario. The parameter of particular interest to us for magma ocean relevance is that the temperature be sufficiently high to render ultramafic silicate completely molten at pressures modest enough for smelting reactions to partially proceed. To generate experimentally such high temperatures without also rendering the silicate liquid composition a strong and unrealistic function of temperature, as would be the case in MgO containers, we used carbon capsules. Graphite saturation experiments have the possible detrimental quality that C activity is invariant and too high and fO_2 is too low to achieve full relevance to Earth's differentiation (e.g., Dasgupta and Walker 2008; Wood and Halliday 2010). We add to the existing body of imperfect Pd and Ag partitioning data by focusing on the effects of very high temperature, sulfur, and variable trace element concentration between the extremes of pure sulfur-free metal and Fe-FeS eutectic endmembers. We combine these new data with existing published data to calculate the ^{107}Ag anomalies expected in mantle plumes for various amounts of core material incorporation. Finally, we compare our experimental partitioning data with those inferred from mantle observations to conclude that there need be no excess mantle siderophile element problem for Pd or Ag.

EXPERIMENTAL METHODS

Detailed descriptions of methods used in this study as well as relevant diagrams are published in Wheeler et al. (2006). The following section summarizes methods used and focuses on aspects unique to this study.

Starting Material

Powdered natural KLB-1 fertile peridotite was combined with powdered Fe and FeS to make roughly chondritic Fe/Si starting compositions with varying S contents. Various mixes of Fe and FeS were prepared to make combined S in the metallic fraction of the starting material be 0, 7, 20, or 28% by mass. These metal fractions were then combined with KLB-1 as mass fractions 0.30, 0.33, 0.39, and 0.42 of the mass of KLB-1 in order to achieve roughly chondritic Fe/Si approximately 1.75. One Ag partitioning experiment (GG958) was instead run with higher Fe/Si at approximately 50 mass% $Fe_{71}Ni_1S_{28}$ metal added to 50 mass% KLB-1 in an effort to increase the analyzable metal surface area in the experimental section. We have no reason to suspect that the increased metal volume or

this different metal composition would affect Ag partitioning behavior. S was chosen as the alloying component because it is highly soluble in liquid Fe, is present in iron meteorites, is hypothesized to be present in Earth's core, affects partitioning behavior in metallic systems (e.g., Jones and Malvin 1990), and can be experimentally varied in abundance. Shavings from pure Pd and Ag wires were added to peridotite KLB-1 + FeFeS mixture as a thin sprinkling near the middle of the sample capsule. Use of this method with U in Wheeler et al. (2006) yielded complete chemical homogenization in each phase under run conditions. Therefore, no additional effort was made to mechanically mix the trace elements with the starting composition. Pd and Ag were added to charges in excess of natural abundances to facilitate analysis in trace-element-poor phases. No special care was taken to ensure that uniform amounts of Pd and Ag were added to each charge, though rough attempts were made to vary concentrations of these elements to assess the effect of their concentration on partitioning behavior.

Assembly

Graphite capsules were used to contain sample material. Graphite was chosen because of its ability, once sintered, to contain molten silicate and sulfide at extremely high temperatures as well as to maintain low oxygen fugacity. These positive experimental attributes come at the cost of the ability to vary carbon activity, so that our experiments are all performed at carbon saturation. The capsules filled with starting material were loaded into high temperature piston cylinder assemblies described in Cottrell and Walker (2006). These assemblies use a $LaCrO_3$ sleeve as a thermal insulator for a graphite heater and thin $BaCO_3$ as a pressure medium. These assemblies facilitated stable and reliable experiments at 2 GPa and 2000–2400 °C for durations of 30 min. Temperature was measured with a type *D* W-Re thermocouple with a junction separated from the capsule by a thin layer of MgO.

Procedure and Equilibrium

The assembly was loaded into a ½ inch Boyd-England piston cylinder apparatus and gradually raised to 2 GPa and 800 °C using the piston-in technique over the course of 45 min. The assembly was allowed to sinter for several hours, typically overnight. Runs that did not incorporate a sintering step characteristically experienced loss of the metallic sulfide phase through porosity in the graphite. Runs that experienced obvious metallic sulfide loss were not included in this study because too little metallic sulfide remained for analysis. Pressure inflation usually accompanied the sintering step and occasionally had to be gently released. This may have introduced error on the order of 10% in the pressure measurement. After sintering, temperature was quickly raised to the final run temperature over the course of several minutes and held for 15–60 min before quench by turning off the power. Residual pressure was released in approximately 20 min. The assembly was recovered from the piston-cylinder vessel, mounted in epoxy, and ground/polished with water using a series of abrasive sizes concluding with 0.3 μ Al_2O_3 grit. Segregation of the initially thoroughly mixed Fe and silicate into separate phases indicates large-scale chemical reorganization. Furthermore, based on diffusion length scales in molten materials at these conditions (Walker and Agee 1989), lack of observed chemical gradients, and complete textural transformation, it is very likely chemical equilibrium was reached in these experiments. Experimental run conditions are detailed in Table 1.

ANALYSIS

The percentage levels of Pd in the metal and ppm levels in the silicate necessitated analysis methods that could successfully detect both high and low element concentrations. For this reason the electron microprobe was used to measure Pd in the metal and the high sensitivity laser ablation inductively coupled plasma–mass spectrometry (LA-ICP-MS) was used to measure Pd in the silicate. Ag partitioned more evenly between the two phases and was usually detectable by both methods. LA-ICP-MS data for Ag was used in this paper because of its capability to analyze large volumes of sample.

Electron Microprobe

Experiments were analyzed both on the Lamont Doherty Earth Observatory's Cameca CAMBAX electron microprobe and on the American Museum of Natural History's Cameca SX-100. Metal, sulfide, and silicate were analyzed with a 15 kV accelerating voltage and a 25 nA sample current. Fifteen second backgrounds were taken with 30 s count times. For metal analyses Fe (Kα) was standardized with Fe metal, S (Kα) with FeS_2, Ni (Kα) with Ni metal, Ag (Lα) with Ag_2S, and Pd (Lα) with Pd metal. For silicate analyses Fe (Kα) was standardized with hematite, Ni (Kα) with Ni metal, Ca (Kα) and Al (Kα) with anorthite, Si (Kα) and Mg (Kα) with enstatite, Cr (Kα) with uvarovite, Ti (Kα) with rutile, La (Lα) and Ba (Lα) with glass CGW, Ag (Lα) with Ag_2S, and Pd (Lα) with Pd metal. Raster mode analysis with fields of view of 10–30 μ^2 was used

Table 1. Run conditions, starting materials, trace element concentrations, and partition coefficients.

Experiment	P (Gpa)	T (°C)	S (wt%)[a]	log fO_2 (ΔIW)	Duration (minutes)	Pd Silicate ppm *SEM* (no. measurements)	Pd Sulfide ppm *SEM* (no. measurements)	Ag Silicate ppm *SEM* (no. measurements)	Ag Sulfide ppm *SEM* (no. measurements)	$D^{\text{metallic sulfide/silicate}}$ (+error, −error)
Pd										
GG973	2	2000	20	−1.8	30	3.4 *0.17* (5)	55217 *697* (9)	–	–	1.6×10^4 (1078, 957)
GG974	2	2100	7	−2.8	30	7.0 *4* (4)	2969 *30* (8)	–	–	4.2×10^2 (575, 156)
GG975	2	2200	7	−3.9	30	45.3 *7* (7)	7191 *61* (9)	–	–	1.6×10^2 (30, 22)
GG977	2	2400	7	−3.4	30	12.7 *1.02* (4)	8322 *60* (8)	–	–	6.5×10^2 (62, 53)
GG959	2	2000	28	−2.88	30	1.7 *0.1* (3)	50561 *1915* (10)	–	–	3.0×10^5 (3151, 2795)
GG948	2	2000	7	−4.15	30	1.6 *0.34* (4)	50574 *3586* (6)	–	–	3.2×10^4 (11416, 7409)
GG942	2	2000	20	−4	30	13.7 *2.5* (4)	32280 *264* (7)	–	–	2.4×10^3 (550, 380)
GG938	2	2000	0	−3.93	60	0.6 *0.03* (5)	89255 *5286* (5)	–	–	1.5×10^5 (16629, 15073)
Ag										
GG939	2	2000	0	−3.55	66	–	–	1.78 *0.06* (5)	256 *9* (4)	1.4×10^2 (10, 10)
GG941	2	2000	20	−3.92	30	–	–	296 *24* (2)	1150 *318* (5)	3.9 (1.5, 1.3)
GG958	2	2000	28	∼ −4	18	–	–	258 (1)	644 *298* (2)	2.5 (1.2, 1.2)

[a]Initially added to the Fe-S fraction of the charge.

to average the heterogeneous quench textures present in both phases. A standard ZAF correction was applied to all data.

Laser Ablation Inductively Coupled Plasma–Mass Spectrometry

The University of Maryland LA-ICP-MS was used to detect ^{107}Ag and ^{109}Ag in the metal and silicate phases and ^{105}Pd in the silicate phase. A Nd:YAG New-Wave UP-213 laser ablation system was coupled to a Thermo Finnigan Element 2 single collector ICP-MS. Most spot sizes were 30–50 μm in diameter with a 5–10 Hz repetition rate. Power density was approximately 6 J cm^{-2}. The guard electrode was turned off to minimize oxide production ($^{232}Th^{16}O/^{232}Th \leq 0.2\%$). Results for both isotopes of Ag were comparable within uncertainties. Three to four analyses were made per phase. NIST610 was used as the standard for both the metal and silicate analyses and it was cross calibrated with an inhouse sulfide standard JB-sulfide (Brenan and McDonough 2009); this use of two reference materials provided critical checks for potential oxide interferences and nonmatrix matching interferences, neither of which were found under these operating conditions. These two reference materials were analyzed before and after the experimental run products, providing the calibration curves to constrain instrument drift and element concentrations. Ni data acquired from the electron microprobe were used as the internal standard for the metal phases while Ca data were used for the silicate. Data were processed off line with Lamtrace software (Longerich et al. 1996).

Most metal and silicate phases were large and thick enough that a sampling on the order of 20–50 s was possible before the laser burned through the sample. (Invariably the laser did burn through the sample. The analysis was surprisingly destructive. Specimens for photography do not remain. Therefore an appreciation of sample appearance and texture must be gained through reference to our previous work on U using the same procedures, i.e., Wheeler et al. [2006], figure 6. The protocol of photographing after analysis was conditioned by nondestructive electron microprobe and earlier LA-ICP-MS analysis where postanalysis photography including the analytical burn made the documentation of analytical coverage unambiguous.) Some metal phases were small and yielded only approximately 5 s of quality signal. For cases when analyses of small metallic blebs matched analyses from larger ones, we considered data from both sizes. When data from the small blebs differed from large blebs consistent with silicate contamination (e.g., high CaO counts), we concluded that silicate material had indeed contaminated the analysis and therefore considered values from large blebs only.

D Value Calculation and Error

Large analytical areas for measurements made with the electron microprobe and LA-ICP-MS in effect average regions of the heterogeneous quench textures of much smaller scale. Bulk compositions of the silicate and sulfide phases were determined by averaging analyses taken on the respective phases. As these analyses represent local averages, uncertainty is best defined by the standard error of the mean (SEM): $\sigma/\sqrt{(n)}$ where σ is the standard deviation of the large-area measurements and n is the number of analyses. $D_M^{\text{metallic sulfide/silicate}}$ was defined as the weight concentration of the element of interest in the bulk metal sulfide ($C_M^{\text{metallic sulfide}}$) phase divided by the concentration in the bulk silicate (C_M^{silicate}). Upper error bounds were defined as $(C_M^{\text{metallic sulfide}} + \text{SEM}_M^{\text{metallic sulfide}})/(C_M^{\text{silicate}} - \text{SEM}_M^{\text{silicate}})$. Lower error bounds were defined as $(C_M^{\text{metal sulfide}} - \text{SEM}_M^{\text{metallic sulfide}})/(C_M^{\text{silicate}} + \text{SEM}_M^{\text{silicate}})$ (Jana and Walker 1998). Electron microprobe measurements were used for measuring Pd concentrations in the Pd-rich metal phase while LA-ICP-MS measurements were used for Pd in the Pd-poor silicate. Ag in the metal was measured with both electron microprobe and LA-ICP-MS, though electron microprobe data were not used for *D* calculation. Electron microprobe measurements of Ag in the metal were close to the detection limit but were of the same order of magnitude as those obtained by LA-ICP-MS. LA-ICP-MS was the preferred analysis technique because it is better suited for averaging dispersed metal and sulfide regions that contained different Ag contents upon quench. The Pd and Ag elemental concentrations measured and Ds calculated in this study are displayed in Table 1. The electron microprobe data are presented in Table 2. In some cases the number of analyses reported is low. This is due to limited phase exposure in some experiments. In addition, the totals of some measurements are significantly below 100%. We did not analyze for *C* and attribute these low totals to its presence.

Correction Procedure

All S-bearing experiments produced two metallic liquid sulfide-bearing phases at the end of runs. The origin of these two phases will be discussed in a following section. Here, we discuss the implications of these phases for *D* value calculations. One phase was S-rich and the other S-poor, approximately 30 wt% S and < 5 wt% S, respectively. Surface area expression of

Table 2. a) Average weight percent compositions of metal measured by EMP. b) Average weight percent compositions of silicate measured by EMP. Error calculated as standard error of the mean (SEM). GG958 was not analyzed by microprobe but was analyzed by LA-ICP-MS. All Ag *D* values were calculated with LA-ICP-MS data.

a.

Experiment	Fe wt%	*SEM*	S wt%	*SEM*	Ni wt%	*SEM*	Pd wt%	*SEM*	Sum	No. measurements
Pd										
GG973	66.67	*2.21*	26.56	*2.80*	0.58	*0.03*	5.52	*0.19*	99.34	9
GG974	94.06	*0.14*	0.43	*0.01*	0.70	*0.01*	0.33	*0.01*	95.52	8
GG975	90.73	*0.55*	0.93	*0.23*	1.05	*0.02*	0.79	*0.02*	93.50	9
GG977	92.17	*0.15*	0.39	*0.06*	0.61	*0.02*	0.92	*0.13*	94.08	8
GG959	69.47	*0.90*	21.87	*1.67*	0.61	*0.03*	8.19	*0.83*	100.14	10
GG948	88.79	*0.31*	0.47	*0.17*	0.61	*0.04*	5.56	*0.89*	95.43	6
GG942	86.25	*1.52*	0.48	*0.03*	0.68	*0.03*	4.44	*0.07*	91.85	7
GG938	87.32	*1.82*	0.02	*0.01*	0.61	*0.0005*	8.93	*0.21*	96.87	2
Experiment	Fe wt%	*SEM*	S wt%	*SEM*	Ni wt%	*SEM*	Ag wt%	*SEM*	Sum	No. measurements
Ag										
GG939	92.03	*0.31*	0.02	*0.01*	0.54	*0.02*	0.07	*0.03*	92.67	10
GG941	92.88	*1.09*	0.27	*0.17*	0.53	*0.03*	0.06	*0.01*	93.75	7

b.

Experiment	SiO_2 wt%	*SEM*	Al_2O_3 wt%	*SEM*	MgO wt%	*SEM*	CaO wt%	*SEM*	TiO_2 wt%	*SEM*	SO_2 wt%	*SEM*	FeO wt%	*SEM*	NiO wt%	*SEM*	Cr_2O_3 wt%	*SEM*	Sum	No. measurements
Pd																				
GG973	44.53	*0.39*	3.57	*0.06*	37.63	*0.43*	3.21	*0.04*	0.14	*0.007*	0.61	*0.49*	12.54	*0.18*	0.03	*0.011*	0.23	*0.009*	102.49	13
GG974	49.27	*0.52*	3.04	*0.04*	40.92	*0.44*	2.56	*0.03*	0.11	*0.005*	1.10	*0.88*	2.55	*0.17*	0.02	*0.008*	0.15	*0.010*	99.72	12
GG975	48.33	*0.41*	2.85	*0.05*	42.18	*0.25*	3.10	*0.02*	0.09	*0.007*	1.76	*1.41*	1.07	*0.08*	0.01	*0.003*	0.09	*0.010*	99.46	12
GG977	47.25	*0.37*	3.06	*0.02*	42.95	*0.25*	3.47	*0.03*	0.10	*0.007*	1.76	*1.41*	1.77	*0.12*	0.03	*0.010*	0.35	*0.022*	100.73	11
GG959	47.82	*0.02*	3.82	*0.03*	42.27	*0.12*	3.35	*0.02*	0.12	*0.004*	1.19	*0.14*	2.67	*0.18*	0.01	*0.006*	0.12	*0.013*	101.38	12
GG948	39.97	*0.20*	1.01	*0.03*	52.03	*0.37*	3.49	*0.05*	0.04	*0.007*	1.27	*0.04*	0.75	*0.04*	0.01	*0.005*	0.07	*0.013*	98.64	8
GG942	44.20	*0.26*	3.70	*0.12*	40.93	*0.26*	4.64	*0.02*	0.13	*0.009*	4.76	*0.10*	0.86	*0.12*	0.01	*0.005*	0.09	*0.010*	99.33	8
GG938	42.80	*0.15*	2.67	*0.02*	44.73	*0.07*	3.69	*0.03*	0.10	*0.005*	n.d.	–	0.95	*0.02*	0.01	*0.003*	0.05	*0.006*	94.99	10
Ag																				
GG939	47.46	*0.53*	3.70	*0.97*	35.69	*3.61*	7.37	*0.23*	0.26	*0.182*	n.d.	–	1.54	*1.08*	0.01	*0.005*	0.22	*0.028*	96.26	10
GG941	47.06	*0.13*	3.04	*0.02*	44.19	*0.14*	3.50	*0.01*	0.14	*0.006*	2.07	*0.09*	1.02	*0.11*	0.02	*0.006*	0.12	*0.014*	101.15	12
GG958	31.31	*0.32*	3.81	*0.16*	34.67	*0.66*	4.61	*0.13*	0.082	*0.007*	3.20	*0.10*	0.27	*0.08*	0.017	*0.007*	0.105	*0.019*	78.08	15

these phases varied depending on how much S was present and on the particular exposed section ground through the charge. Sometimes, only one phase was visible in a particular section, though this did not exclude the presence of the other phase. Pd and Ag partition differently between the S-rich and S-poor phases. Pd slightly prefers the sulfide at sulfur contents below 20 wt% and concentrates in the metal at higher sulfur contents. Ag, in contrast, partitions heavily into the S-poor metal phase with increasing intensity with higher sulfur concentrations from 3 to 31 wt% S (Chabot and Drake 1997). The differing partition behavior renders neither phase representative of the true Pd or Ag content of the metallic phase as a whole. When only one phase was visible, we applied a correction procedure using Ag and Pd partitioning data between solid Fe and metallic liquid in the Fe-FeS system from Chabot and Drake (1997) combined with the measured composition and expected relative proportions of the two phases. Initial S content of the charge and microprobe data of the exposed phases were used to calculate the relative proportions of S-rich and S-poor phases. Trace element content for the nonexposed phase was calculated with the exposed phase's observed composition and the trace element's S-rich to S-poor partitioning behavior. This procedure was tested with experiment GG959, which had exposures of both metal and sulfide phases. Using values from the S-poor phase, the procedure correctly calculated the Pd content of the S-rich phase. The additional error that this correction introduces is minimal due to the small error range (approximately 10%) in the metal/sulfide partition coefficients of Chabot and Drake (1997). This error is included in the total measurement error in Table 2. The correction procedure was used for Pd in the metal phases only. It was not used for Ag in the metal because, as mentioned above, Ag was measured with LA-ICP-MS which measures deep into the sample, thereby averaging a more complete ensemble of both metallic liquid phases. It should be noted that Chabot and Drake's (1997) Ds are measured between solid metal and liquid sulfide, not between liquid metal and liquid sulfide as present in this study. The extent to which these two systems differ will affect the accuracy of our correction procedure.

RESULTS

Run Products

Upon melting, the KLB-1 + Fe-FeS mixture segregated into a volumetrically dominant molten silicate phase and complementary metal phases clustered as blobs on the capsule walls. The silicate quenched to Mg-rich spinifex olivine laths separating residual Ca and Al-rich glass. Within the Ca and Al-rich glass were metallic blebs that were particularly prevalent in high-S runs. The small blebs and the bigger blobs are well illustrated in figure 6 of Wheeler et al. (2006), a companion study of U partitioning. The small blebs are spherical and several microns to submicron in size. They tend to be restricted to the glass or glass-lath interfaces and not to occur within the laths. They are also unlike the larger, aspherical liquid metal blobs on the capsule margins, which dimensionally can be 10 s–100 s of microns across, in that there is no preference for the small blebs to be found near the graphite capsule walls. Such blebs have been previously reported and interpreted from chemical and textural evidence as Fe-FeS-rich quench exsolutions from the silicate liquid (e.g., Fleet et al. 1991; Jana and Walker 1997; Wheeler et al. 2006). In this study, based on their low siderophile element concentrations, we also interpret these blebs as silicate quench products and made no effort to exclude them from silicate analyses.

The metallic phase of S-bearing experiments consisted of S-rich and S-poor regions each of which quenched to a dendritic intergrowth of metal crystallites plus interstitial crystalline sulfide. We interpret these textures as evidence for immiscible melts. The two regions, each comprised of dendrites and interstitial material in different proportions, had mutual droplet-in-blob textures suggestive of liquid-state immiscibility. This texture was encountered previously in the analogous U partitioning experiments reported by Wheeler et al. (2006) who provided photomicrographs of this texture in their figure 6. There, the texture was interpreted as the product of exsolution of an Fe-rich liquid and a residual sulfide liquid each of which subsequently crystallized to Fe dendrites in troilite on quench. It was not known whether the immiscibility was stable at experimental P–T or whether it was introduced on quench. The same ambiguity is encountered here along with the same evidence that there are indeed two immiscible metallic sulfide liquids. The evidence for separate liquid compositions is presented in Fig. 1. Here, sulfide Pd content is plotted against sulfide S content for a set of 2k small raster electron microprobe analyses of GG959, a high-S experiment. It is immediately clear from this figure that there are two distinct compositional arrays. There is a narrowly defined low-S sulfide with 0–4% S and 5–8% Pd and a loosely defined high-S sulfide with 5–35% S and 1–14% Pd. The large spread of S and Pd contents in the high-S sulfide is consistent with the fine-scale dendritic crystallization of a high Fe and high Pd quench metal and interstitial high S and low Pd residual sulfide liquid. The low-S sulfide does not exhibit such a dramatic compositional spread because

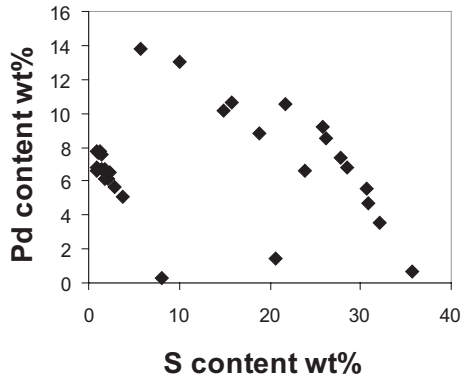

Fig. 1. Two quench-induced metal fractionation arrays of Pd versus S from experiment GG959. These arrays suggest that two metallic sulfide liquids were present in experiments. Upon quench, these phases further segregated into Fe-rich and S-rich endmembers. These two arrays could result from two immiscible liquids stable at experimental *P–T*. Alternatively, it is not possible to completely rule out that they could have formed during the early stages of quenching. Fe-rich solids crystallized with progressively falling T from each immiscible liquid. The data in this figure were acquired specifically to understand the chemical variability in quenched phases. They differ from the data for GG959 reported in Tables 1 and 2 which are from larger analytical areas that average the compositional variability within those phases.

the low S content allows only comparatively small volumes of residual sulfide liquid to form on quench. The presence of two distinct Fe-FeS phases in these experiments is evidence for an expanded Fe-FeS solvus at these P, T, and X conditions. Carbon from the capsule may promote this immiscibility which is not present stably in the Fe-FeS system, even though such immiscibility must be very close to stable at low pressure given the unusual curvature of the Fe-FeS liquidus for Fe (Walker and Li 2008). Perhaps Pd may be involved in inducing this immiscibility, but Pd partitions itself relatively indifferently between S-rich and S-poor phases, at least at atmospheric pressure and 1150–1450 °C (Chabot and Drake 1997) and also here in experiments like GG959 where Fig. 1 shows the Pd contents in the two liquid phases to be overlapping. Thus, assuming the relevance of the Chabot and Drake (1997) data, consistent with our Fig. 1, the correction we apply to the Pd data for the two-metal aggregate weighted for phase abundance and composition has a minimal impact on our *D* values. Therefore, it is not critical to our reported Ds for Pd whether this solvus is metastable, and only encountered during quenching, or stable at experimental *P–T* as our textural interpretation suggests. It is important to remember that, in the context of Pd *D* metal/silicate always above 160, small fractionations between the metal phases are trivial.

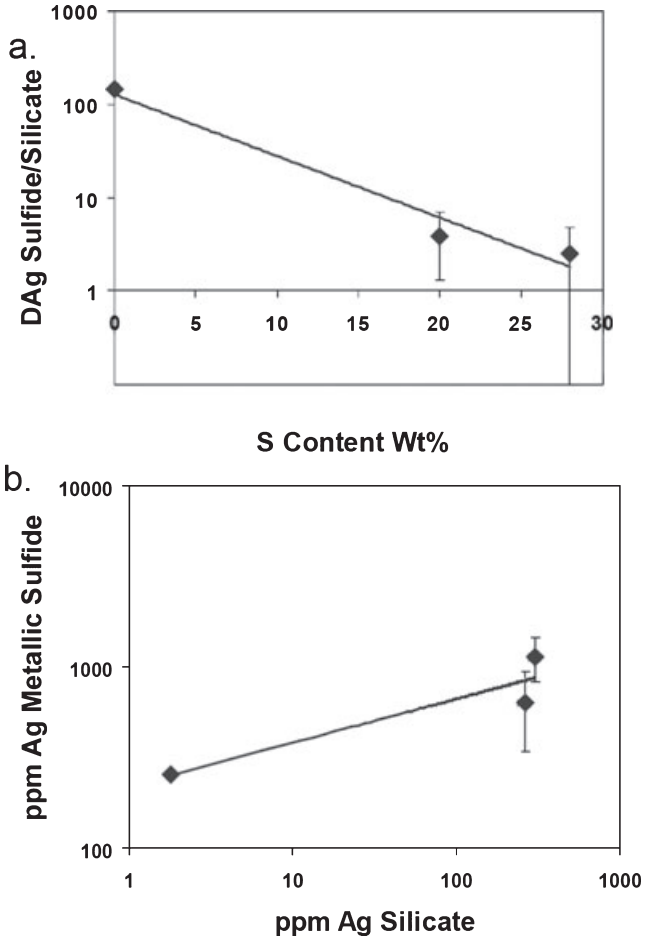

Fig. 2. Ag partitioning results from this study. a) $D_{Ag}^{\text{metallic sulfide/silicate}}$ decreases with increasing experimental S content (S wt% is the S added to the metal starting mix). b) Silicate Ag contents increase with metallic sulfide Ag contents with a positive log–log slope of 0.24, unlike Pd which decreases in silicate as Pd in metallic sulfide rises. The S contents of the starting metal do not track with Ag content, suggesting that S is the significant variable affecting $D_{Ag}^{\text{metallic sulfide/silicate}}$ in part (a), not Ag concentration. This is unlike the case for Pd to be presented below.

Partition Coefficients of Pd and Ag

Experimental results are plotted in Figs. 2 and 3. The values in these figures are tabulated in Table 1. Ag displays relatively simple partitioning systematics with S content (Fig. 2a). It is siderophile for lower S contents explored in this study but displays S-avoidance of the type described for Cr by Jones and Malvin (1990). $D_{Ag}^{\text{metallic sulfide/silicate}}$ is highest at approximately 1.4×10^2 with 0 wt% S, decreases to approximately 3.9 at 20 wt% S, and finally falls to approximately 2.5 at 28 wt% S, where wt% S is the S added to the metal starting material. The data

can be fit by an exponential curve, not adjusted for error, for $D_{Ag}^{\text{metallic sulfide/silicate}}$ variation with S:

$$D_{Ag}^{\text{metallic sulfide/silicate}} = 126e^{-0.15*Xs} \quad (1)$$

The exponential relationship between $D_{Ag}^{\text{metallic sulfide/silicate}}$ and S added to the metal is uncertain due to large uncertainties at high S content. These large errors could stem from Ag heterogeneities in the immiscible metallic phases. From 0 wt% S to 20 wt% S, $D_{Ag}^{\text{metallic sulfide/silicate}}$ declines 2 orders of magnitude, well outside the bounds of the uncertainty. However, distinguishing between $D_{Ag}^{\text{metallic sulfide/silicate}}$ at 20 wt% S and 28 wt% S is not possible within error. Whether the relation between D_{Ag} and S content of the starting material should be exponential or some other functional form is also uncertain. Different forms would predict different D values in the poorly covered 0–20% S range, a point to which we return below.

Ag content in the silicate increases with Ag content in the metallic sulfide. The data may be fit on a log–log plot (Fig. 2b) as follows:

$$\text{Ag ppm in silicate} = 220 \times (\text{Ag metal ppm})^{0.24} \quad (2)$$

The Ag data in Tables 1 and 2 reveal that the trend in Fig. 2b does not track S content. Indeed, in contrast to Pd, there is no clear relationship between total experiment Ag content and $D_{Ag}^{\text{metallic sulfide/silicate}}$.

$D_{Pd}^{\text{metallic sulfide/silicate}}$ responds differently to S content added to the metal than $D_{Ag}^{\text{metallic sulfide/silicate}}$ (Fig. 3a). $D_{Pd}^{\text{metallic sulfide/silicate}}$ varies from approximately 150 to approximately 15,000 without defining a clear trend, indicating that Pd partitioning behavior is not primarily dependent on S. Similarly, T does not significantly impact $D_{Ag}^{\text{metallic sulfide/silicate}}$. Figure 3b illustrates $D_{Pd}^{\text{metallic sulfide/silicate}}$ against T for experiments with identical 7 wt% S contents added to the metal. Most of the data cluster in the 10^2–10^3 range with no systematic variation in temperature. What is evident from examining the data subsets in Figs. 3a and 3b is that high Pd concentration in the metallic sulfide phases tends to correspond to high $D_{Pd}^{\text{metallic sulfide/silicate}}$. This relationship is more clearly seen in Fig. 3c. All the Pd data from this study are included on this plot. They lie along an approximately linear trend on a log–log plot that increases 2 orders of magnitude from approximately 150 at low concentrations of Pd in the metal to approximately 15,000 at high concentrations demonstrating $D_{Pd}^{\text{metallic sulfide/silicate}}$ dependence on experimental Pd content. A power law trendline fits the data well with a R^2 value of 0.84 and the equation:

$$D_{Pd}^{\text{metallicsulfide/silicate}} = (5 \times 10^{-5}) \times (\text{Pd metal ppm})^{1.8} \quad (3)$$

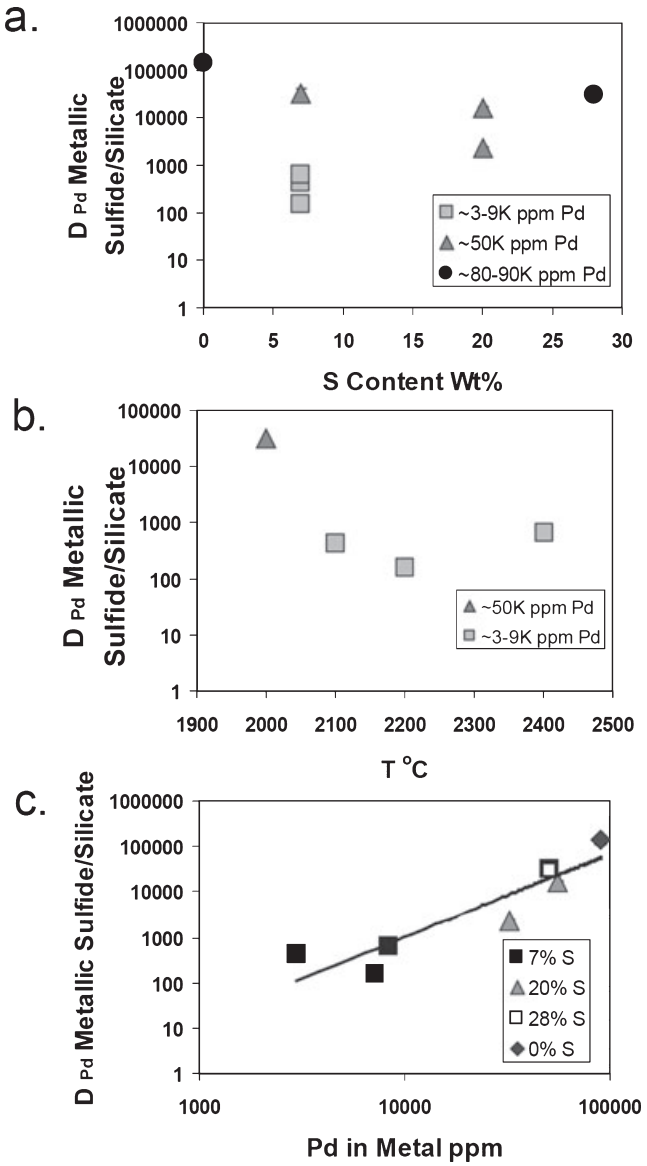

Fig. 3. This study's Pd results. a) $D_{Pd}^{\text{metallic sulfide/silicate}}$ does not display a coherent relationship with S content (S wt% is the S added to the metal starting mix). b) $D_{Pd}^{\text{metallic sulfide/silicate}}$ does not vary with T in experiments with similar Pd contents. c) $D_{Pd}^{\text{metallic sulfide/silicate}}$ varies systematically with Pd content in the metal phase, particularly at high (> 1 wt%) Pd contents.

The uncertainty in these data is smaller than the plotted symbols.

DISCUSSION

Ag: Comparisons with Previous Study

The only other measurement of $D_{Ag}^{\text{metallic sulfide/silicate}}$ of which we are aware is that of Jones and

Drake (1986). Their value of approximately 100 at 23–27 wt% S is much higher than this study's $D_{Ag}^{\text{metallic sulfide/silicate}}$ of approximately 3 at similar S contents. In our experiment with pure metal and no S, the $D_{Ag}^{\text{metal/silicate}}$ is of the same order of magnitude as Jones and Drake's high S value. However, differences increase sharply with increasing S content. The reason for this difference is not well constrained. The differences between this study and the work of Jones and Drake are numerous and could account for the discrepancy. Our pressures and temperatures are higher, with 2 GPa and 2000 °C in this study versus atmospheric pressure or lower and 1250 °C in theirs. We used high-NBO/T KLB-1 as our silicate compared to Jones and Drake's more polymerized synthetic basalt. Two of our three experiments contained little Ni while theirs contained significant amounts. Finally, our oxygen fugacities were significantly lower: about four log units below IW versus theirs at QFM. There are so few published $D_{Ag}^{\text{metallic sulfide/silicate}}$ partitioning data that it is difficult to identify any one factor as the cause of the differences.

When applied to the excess siderophile element problem, data from both this study and Jones and Drake (1986) draw the same conclusion (Fig. 4). Observed mantle abundance of Ag is on the order of 10^{-1} to 10^{-2} relative to CI chondrites. Entering a range of $D_{Ag}^{\text{metallic sulfide/silicate}}$ calculated from S contents of 5–10 wt% S in Equation 1 and using bulk Earth and CI Ag contents of McDonough (2003) and Palme and Jones (2003) respectively, we calculated mantle Ag depletion (0.1–0.05) that overlaps the observed range of uncertainty-bounded Ag concentration. The same calculation using Jones and Drake's (1986) $D_{Ag}^{\text{metallic sulfide/silicate}}$ of 100 yields a depletion of 0.03, also consistent with mantle observations. It should be noted that the fO_2 of this study's experiments (ΔIW-4) lies below the most widely accepted value for the magma ocean (ΔIW-2, e.g., Righter and Drake 1999), and the 23–27 wt% S content of Jones and Drake (1986) lies above plausible magma ocean metallic sulfide S contents.

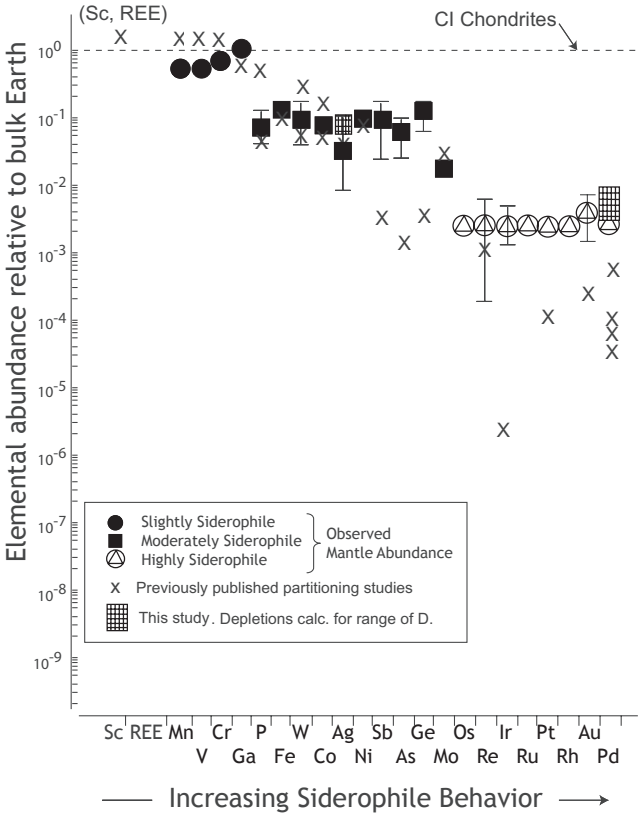

Fig. 4. Elemental abundances relative to bulk Earth and CI chondrite. Adapted from Righter and Drake (1997), Drake and Righter (2002), and Cottrell and Walker (2006). Solid circle, solid square, and triangle-in-circle symbols represent observed mantle depletions from McDonough and Sun (1995). These values were volatility corrected in Righter and Drake (2003) by comparison to lithophile/volatile depletion trends according to Newsom and Sims (1991). The "x" symbols represent depletions calculated from literature experimental data. No graphical distinction is made for the specific experimental conditions of these data. Experimental values for phosphorus, tungsten, cobalt, nickel, molybdenum, rhenium, and gallium were selected from the high pressure and temperature experiments of Righter and Drake (1997, 1999, 2000); Pt from Cottrell and Walker (2006); Ag from low pressure work of Jones and Drake (1986); Pd from high and low pressure experiments and extrapolations of Holzheid et al. (2000), Crocket et al. (1997), and Fleet et al. (1999). The remaining experiments were selected from the data of Newsom (1990), Newsom et al. (1996), and Capobianco et al. (1993). Error bars are from the above-cited studies. Agreement between observation from the mantle and expectation from experiment is particularly poor for the highly siderophile elements (HSEs) and some moderately siderophile elements (MSEs). The reasonable mantle depletion ranges for Pd and Ag partitioning data of this study (hatched zones) were calculated using the $D^{\text{metallic sulfide/silicate}}$ values of this study (D_{Ag} from experiments with 5–15 wt% added S and D_{Pd} from experiments with 3000–9000 ppm added Pd) and bulk Earth Pd and Ag values of McDonough (2003) and Palme and Jones (2003). The experiments from this study's most magma-ocean relevant experiments overlap observed mantle depletions for Pd and Ag.

Pd: Comparisons with Other Studies

The 150 to 15,000 span found in this study's $D_{Pd}^{\text{metallic sulfide/silicate}}$ data overlaps the bulk of the 480 to 2×10^7 spread of published data (Fig. 5). The highest $D_{Pd}^{\text{metallic sulfide/silicate}}$ from this study, approximately 15,000, comes from a S-free experiment and agrees well with T-extrapolated values from other S-free studies by Borisov et al. (1994) and Holzheid et al. (2000). Although the Borisov and Holzheid studies are based on solubility experiments rather than two-phase partitioning, the Pd contents in their silicates are on the same order as those

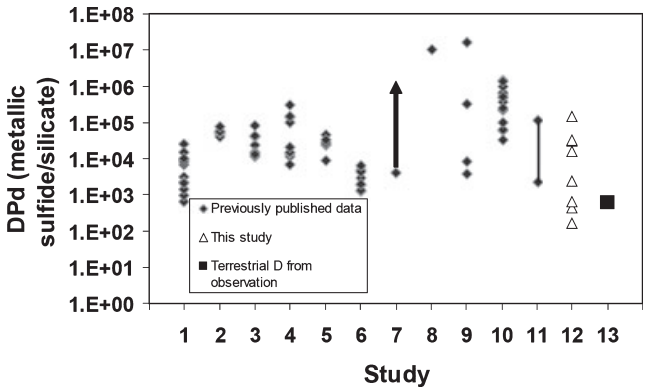

Fig. 5. The range of published data in graphical form. The sources for the table data are (1) Fleet et al. (1991). (2) Bezmen et al. (1994). (3) Peach et al. (1994). (4) Fleet et al. (1996). (5) Crocket et al. (1997). (6) Fleet et al. (1999). (7) Sattari et al. (2002). (8) O'Neill et al. (1995). (9) Borisov et al. (1994). (10) Holzheid et al. (2000). (11) Righter et al. (2006, 2008). (12) This study. (13) Value of D inferred if the mantle is to be an equilibrium separation product of the core, given an Earth Pd composition of 1 ppm. McDonough (2003).

in this study. The $D_{Pd}^{metallic\ sulfide/silicate}$ data from this study also agree with experiments reported in Righter et al. (2006, 2008). At similar Pd contents, pressure and graphite capsules, Righter et al. (2006, 2008) observe $D_{Pd}^{metallic\ sulfide/silicate}$ to range from approximately 10,000 to approximately 40,000, overlapping values in our study. Furthermore, Righter et al. (2006, 2008) report a low $D_{Pd}^{metallic\ sulfide/silicate}$ of 480 (± 80) which overlaps the lowest values of this study. However, Righter et al. (2006, 2008) attribute their low $D_{Pd}^{metallic\ sulfide/silicate}$ to a pressure effect, while we attribute it to lower experimental Pd contents.

Righter et al. (2006, 2008) have parameterized Pd partitioning. While the Righter et al. (2006, 2008) parameterization seems to fit the bulk of Pd data quite well, close inspection reveals complexity. The S-free Pd solubility data of Borisov et al. (1994) and Borisov and Palme (1996) define a coherent trend. However, the S-bearing data from Stone et al. (1990) and Fleet et al. (1996), while lying within the 2σ error bounds of Righter et al's. (2006, 2008) parameterization, form a trend running at a sharp angle to the aforementioned S-free solubility data. The S-bearing experiments from this study form a subparallel trend to S-bearing experiments of Stone et al. (1990) and Fleet et al. (1996) identifying another case in which the Righter et al. (2006, 2008) parameterization is not able to explain the details of $D_{Pd}^{metallic\ sulfide/silicate}$ variation in S-bearing systems.

Some light can be shed on $D_{Pd}^{metallic\ sulfide/silicate}$ variability by approaching it from the perspective of silicate solubility surfaces in the metallic sulfide–silicate Pd ternary. This hypothesis provides a conceptual framework by which interlaboratory variation can be explained. The details are discussed below.

Trends

Insignificant Factors

Though in conflict with many previous findings, fO_2 was not observed to significantly affect $D_{Pd}^{metallic\ sulfide/silicate}$ in this study. fO_2 ranged from -1.8 to -4.0 log units below IW with most experiments falling in the -3 to -4 range. The range of fO_2 in this study is comparable to much of the existing work on this system and perhaps does not cover a wide enough range to emphasize any fO_2 variation that might be present. Our fO_2s were calculated relative to the iron-wüstite (IW) buffer using the methods of Hillgren et al. (1994). At the temperatures used in this study, which are well above the melting points of either iron or wüstite, the IW buffer has marginal meaning. Hillgren's method for calculating relative fO_2 values based on FeO in the silicate and Fe in the metal, is an adequate but necessarily qualitative guide. More sophisticated calculations based on more complex solution models based at much lower temperature are not justified here. The silicate phase KLB-1 contained roughly 8 wt% FeO at the beginning of the experimental run but often finished the experiment with only 1–2 wt% with the missing Fe presumably taken up by the metal phase. This low silicate FeO content is well below mantle value of 6–8 wt%, suggesting that this study's conditions were more reducing than a realistic magma ocean (e.g., Hirose and Kushiro 1993). The O liberated from the silicate could have been consumed by the graphite capsule or some other undetermined O-sink. Two experiments, GG958 and GG973, exhibited anomalously high FeO (approximately 12 wt%); the reason for this high value remains unclear. The source of oxidation in these experiments has not yet been identified but could have come from an imperfectly sealed capsule. Another experiment, GG942, showed a very high silicate S content. The reason for this also remains unexplained. Regardless, no effect of fO_2 was observed on $D_{Pd}^{metallic\ sulfide/silicate}$ over the small range of fO_2 covered in this study.

Temperature, despite a 300 °C experimental range at a single S composition (7 wt%), also had no observable effect on $D_{Pd}^{metallic\ sulfide/silicate}$ (Fig. 3b). In contrast, the Pd solubility studies of Borisov et al. (1994), O'Neill et al. (1995), and Holzheid et al. (2000) all show strong negative T-dependence in $D_{Pd}^{metallic\ sulfide/silicate}$ due to increasing Pd contents in the silicate with T. The T-responsive trend is consistent with Pd dissolved in the silicate either as a metal or as a metal

complex behaving as a metal. Righter et al. (2006, 2008) also observe a decrease in $D_{Pd}^{metallic\ sulfide/silicate}$ with increasing temperature. However, this trend only occurs in experiments contained in MgO capsules, potentially due to increasing depolymerization of the silicate melt with increasing temperature. In experiments contained in graphite capsules, Righter et al. (2006, 2008) report no change in $D_{Pd}^{metallic\ sulfide/silicate}$ with temperature. We are not aware of a published relationship between $D_{Pd}^{metallic\ sulfide/silicate}$ and T in S-bearing experiments. We must leave open the possibility that rapid chemical re-equilibration upon quench could cause phases to reflect a closure temperature lower than that of our high-T experimental run conditions, thereby altering any signature that may have existed at high temperature.

Fleet et al. (1991) were the first to suggest that S content negatively correlates with $D_{Pd}^{metallic\ sulfide/silicate}$. However, Fleet et al. (1999) reported the opposite. It is difficult to confidently separate the effects of metal or silicate S content on $D_{Pd}^{metallic\ sulfide/silicate}$ from those of Pd concentration and fO_2 in the data of Fleet et al. (1991). Similarly, data of Fleet et al. (1999) display only a weak trend. It should be noted that metal S contents of these studies cluster near the eutectic and span very little compositional space, leaving open the possibility for greater $D_{Pd}^{metallic\ sulfide/silicate}$ variation with greater variation in S content. In fact, plotting $D_{Pd}^{metallic\ sulfide/silicate}$ against metal S content for the data of Peach et al. (1994) reveals a decrease in $D_{Pd}^{metallic\ sulfide/silicate}$ by a factor of 4 with increasing S content from 33 to 38 wt% in the metal. Our study, however, explores S content from 0 to 28 wt% in the metal and reveals no discernable trend. Whether this is because there is no effect or simply because the effects are overshadowed by another factor is undetermined. It is still unclear the extent to and means by which Pd complexes with S in the silicate and metallic melts.

Pd Concentration

In contrast to the unclear trends discussed previously, susceptibility of $D_{Pd}^{metallic\ sulfide/silicate}$ to experimental Pd concentration in the FeFeS-silicate system is better documented. However, adjustment using this factor alone fails to facilitate robust interstudy agreement. Evidence for Pd concentration influencing $D_{Pd}^{metallic\ sulfide/silicate}$ can be seen in Fig. 6a. Pd concentration in the metal phase, essentially the total Pd in the experiment, is plotted against $D_{Pd}^{metallic\ sulfide/silicate}$ for a number of Pd partitioning studies. The data of Fleet et al. (1991), Crocket et al. (1997), this study, and possibly Fleet et al. (1999) display a positive correlation between $D_{Pd}^{metallic\ sulfide/silicate}$ and Pd concentration in the metal, albeit at different slopes. This is consistent with a silicate "saturating" with Pd and the

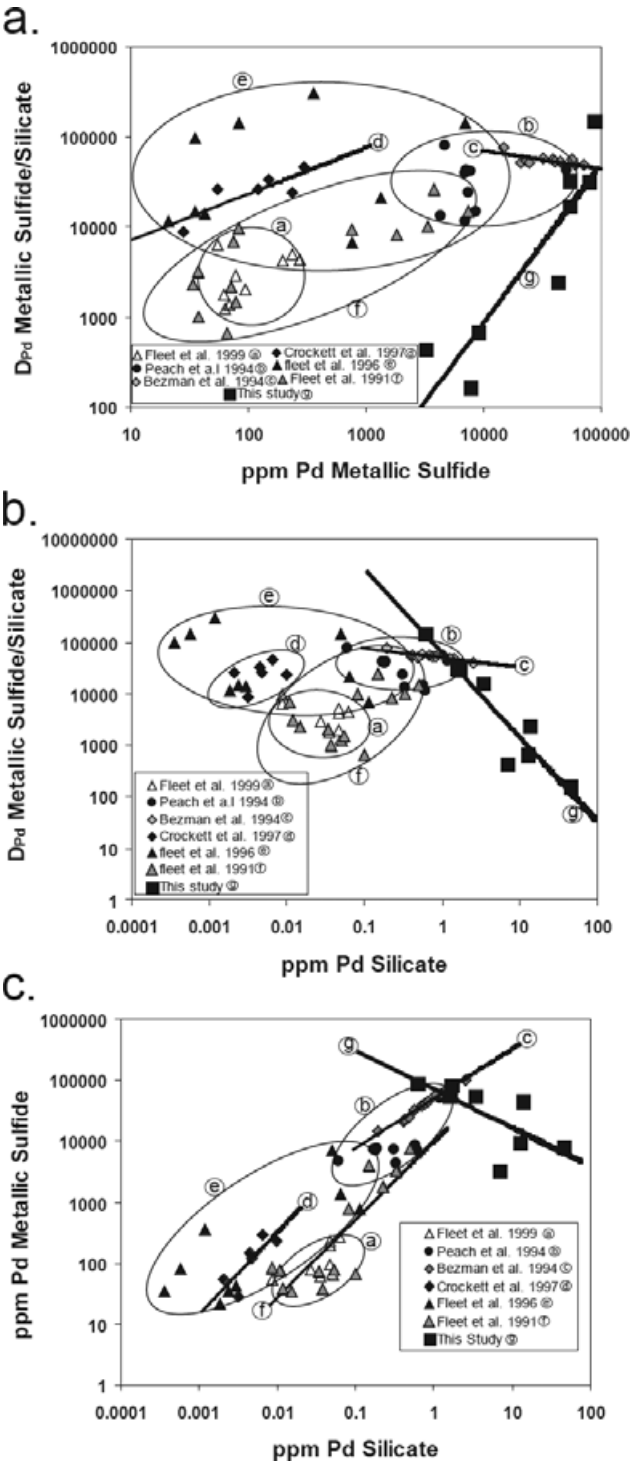

Fig. 6. a) $D_{Pd}^{metallic\ sulfide/silicate}$ values for this study and others as they vary with Pd content in the metal, a proxy for total experimental Pd. The data from this study trend in the same sense as do the rough fits of some of the other data, however the slopes differ. b) $D_{Pd}^{metallic\ sulfide/silicate}$ varies also with the Pd content of the silicate. c) Disturbingly, metallic sulfide and silicate Pd contents from this study anticorrelate. This trend is not observed in other studies and it contrasts with Fig. 2b of this study for Ag.

excess entering the metal phase. Contrastingly, the data from Bezmen et al. (1994) show a slight anticorrelation of these variables.

Though several studies display the Pd concentration-$D_{Pd}^{metallic\ sulfide/silicate}$ correlation, these trends fail to bring the disparate data of Fig. 6a into concert for several reasons. First, the slopes of the trends differ significantly among studies. The Fleet and Crockett studies have modest slopes with $D_{Pd}^{metal/silicate}$ increasing approximately 1 order of magnitude for every 2 orders of magnitude increase in metal Pd content. However, the $D_{Pd}^{metallic\ sulfide/silicate}$ data from this study increase approximately 2 orders of magnitude for every order of magnitude increase in metal Pd content, a factor of 4 greater than in the other studies. The Bezmen et al. (1994) data actually decrease, though gradually, with a $D_{Pd}^{metallic\ sulfide/silicate}$ drop of 1 order of magnitude for every 4 orders of magnitude increase in metal Pd content.

Second, extrapolations of Pd concentration-$D_{Pd}^{metallic\ sulfide/silicate}$ trends from high-Pd studies (e.g., Bezmen et al. 1994 and this study) do not coincide with studies conducted at lower Pd contents (e.g., Fleet et al. 1991 and Crocket et al. 1997). However, all studies seem to converge at $D_{Pd}^{metallic\ sulfide/silicate}$ of 10^5 with metal Pd contents of 10^5 ppm. That these trends do not account for the differences among studies suggests that there is another important factor (or factors) influencing Pd partitioning behavior. One suspect is the configuration of the metallic sulfide–silicate Pd ternary and its potential sensitivity to T and composition differences among studies. We will revisit this issue below.

The data of this study and some others display clear correlation between Pd concentration and $D_{Pd}^{metallic\ sulfide/silicate}$. Sensitivity of $D_{Pd}^{metallic\ sulfide/silicate}$ to Pd concentration is not unexpected, but some of the details are. A system with a Pd-saturated silicate should exhibit a $D_{Pd}^{metallic\ sulfide/silicate}$ increase as additional Pd enters the system and partitions preferentially into the metal. This positive correlation is seen for all studies plotted in Fig. 6a, except for Bezmen et al. (1994) and Righter et al. (2008), although the Righter et al. (2008) data is comprised of three individual 3-point and 4-point subsets at very different experimental conditions that show no particular trends. In this ''the-silicate-is-filling-up'' scenario, the silicate Pd content might be expected to either increase or stay the same as more Pd is added. This is more or less the case for the various studies of the Fleet group. However, this is not the case for those studies done at higher concentration of Pd. As can be seen in Fig. 6b, the Pd content of the silicate actually *decreases* with increasing $D_{Pd}^{metallic\ sulfide/silicate}$ for Pd concentrations in excess of 0.1 ppm in the silicate. Although the disparate individual subsets of Righter et al. (2008) do not show this decrease, taken together, these three subsets show a decreasing trend of silicate Pd as D increases. This observation challenges the rationale that $D_{Pd}^{metallic\ sulfide/silicate}$ increases as the silicate fills, at least at high Pd concentration. It is not that $D_{Pd}^{metallic\ sulfide/silicate}$ rises because the extra Pd goes preferentially in the metal, it is that the Pd is preferentially and increasingly excluded from the silicate. There must be some additional mechanism beyond the-silicate-is-full to raise $D_{Pd}^{metallic\ sulfide/silicate}$.

Another unexpected aspect of the departure from the expected Pd concentration-$D_{Pd}^{metallic\ sulfide/silicate}$ relationship can be seen in Fig. 6c. One expects the activity of an ingredient to be correlated with its concentration. That is the basis of the Nernstian D formulation. Therefore one expects in a system for which the D formulation is relevant, that increasing the concentration of a partitioned substance in one phase should boost the concentration proportionately in the other phases with which it is in equilibrium. Indeed the Pd concentrations in the metal and silicate liquids positively correlate with one another in most studies shown in Fig. 6c. The disparate subsets of Righter et al. (2008) individually show little such correlation but their aggregate does show a positive correlation. Our work in Fig. 6c trends oppositely to all previous work in this respect. Henry's Law clearly is as irrelevant as D to systems showing this bizarre sort of behavior.

We believe these two trends illustrated by our data in Figs. 6b and 6c are related to one another. The schematic metallic sulfide-silicate Pd ternary system (Fig. 7a) provides a plausible framework for explanation of this apparently paradoxical behavior. The key lies in the curved form of the silicate saturation surface (inset). As dissolved metallic Pd in the metal sulfide liquid increases, Pd and other metallic ingredients in the silicate proceed along a complex variation illustrated as a ternary phase compatibility diagram at an arbitrary T–P near the experimental conditions. Pd concentration in the silicate liquid increases to a maximum and then tapers off toward the silicate-rich corner of the ternary as total Pd increases in the system. This configuration, depicted schematically in Fig. 7a, yields the requisite decrease in silicate Pd with increasing Pd in the metallic sulfide at high Pd contents, and the expected increase in silicate Pd with increasing metallic sulfide Pd at low total Pd concentrations. Reference to Fig. 6c suggests that Pd in excess of 1 ppm in silicate is a region beyond the bounds of Henrian behavior.

If the working hypothesis depicted in Fig. 7 is confirmed, it may be time to move beyond D in

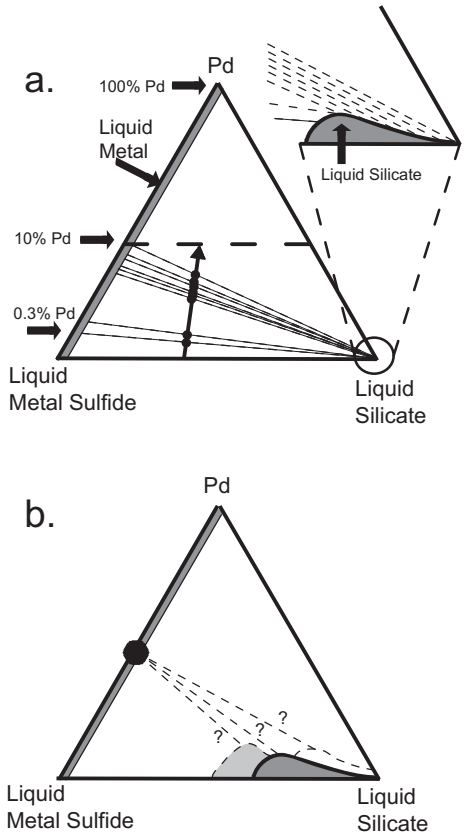

Fig. 7. Ternary diagrams presenting possible explanations for the surprising data trend in this study and interstudy variation in $D_{Pd}^{metallic\ sulfide/silicate}$. a) Curvature in the silicate Pd saturation surface can explain this study's decreases in silicate Pd content with overall experimental Pd increases. b) A silicate Pd saturation surface whose shape and extent is sensitive to variable experimental conditions could provide explanation for interlaboratory differences.

geochemical modeling in the way that igneous petrology has moved beyond freezing point depression to model silicate liquidus systems. Likewise, the use of regression analysis to discover *D* systematics may produce results that would be as useful as using regression analysis would be to model liquidus surfaces.

Curvature of saturation surfaces has been invoked by other workers to explain chemical trends in metallic sulfide–silicate systems. Jana and Walker (1997) use curvature of the silicate saturation surface in the Fe-S-silicate ternary to explain a decrease in silicate S with increasing overall experimental S content. Jana and Walker (1997) attribute the curvature to compositional variability in activity coefficients of sulfur-bearing species. These observations provide little insight into which physical or speciation effects drive them, and must be considered more of a rationalization than an explanation. Likewise the curved saturation surface only forms the basis of a working hypothesis in the present study; a delineation of the various underlying G-X surfaces is inaccessible with present information (where G refers to Gibbs free energy).

In addition to providing a plausible working hypothesis for decreasing silicate Pd contents, the metallic sulfide–silicate Pd ternary is a useful conceptual framework to address interlaboratory variations in $D_{Pd}^{metallic\ sulfide/silicate}$. The important issue here is that the silicate Pd solubility surface may change form, possibly in complicated ways, in response to variations in physical and chemical conditions. A silicate solubility surface under one set of P, T, and X conditions may be very different from one under another set of conditions. The result would be different silicate Pd contents for given total system Pd contents thereby altering the outcome of $D_{Pd}^{metallic\ sulfide/silicate}$ calculations. A schematic representation of this idea is presented in Fig. 7b.

The degree to which P, T, and X affect the silicate Pd solubility surface is not well known. However, as discussed above, the surface is potentially sensitive to T, fO_2, and compositional variables. If this is true across the extent of the silicate Pd solubility surface, conducting good early Earth-relevant experiments depends crucially on imposing appropriate experimental conditions. If incorrect conditions are imposed and they affect the solubility surface, then the resulting Ds measured could be very much in error.

The silicate composition, S content, metal fraction, and fO_2 of our experiments were chosen in an attempt, as discussed in the Experimental Methods section, to best reflect those of a magma ocean scenario on Earth. The P and T variables were chosen more out of experimental necessity than consideration for faithful representation of a magma ocean. Many other studies (e.g., Fleet et al. 1991; Crocket et al. 1997; etc.) were conducted under conditions applicable to sulfide deposit formation and are therefore not strictly applicable to the environment of early Earth and a deep magma ocean. In these and other studies, the silicate compositions are more polymerized and S contents are at or near the eutectic (Table 1). It is therefore of little surprise that the results of this study differ so markedly from the published body of literature. One exception to this generalization is the work of Righter et al. (2006, 2008) that, using depolymerized silicate melt at 1.5–15 GPa, 1500–2150 °C obtain a $D_{Pd}^{metallic\ sulfide/silicate}$ of approximately 480, which is in close agreement with the results presented here.

So what $D_{Pd}^{metallic\ sulfide/silicate}$ values are the most representative of planetary differentiation occurring in a magma ocean? The answer would lie in experiments that best represent the chemical and physical conditions

of early Earth. Unfortunately, there are no experiments to date which faithfully do so. This study imperfectly emulates the bulk compositional conditions that would have existed in a magma ocean and incorporates unrealistically high concentrations of Pd. Our low oxygen fugacity leads to an experimental silicate more depleted in FeO than the actual mantle. Furthermore, as there is a demonstrated relationship between Pd concentration and $D_{Pd}^{metallic\ sulfide/silicate}$ in this system, the application of our data is limited. Most other work, on the other hand, employs very low concentrations of Pd and therefore reduces effects associated with high Pd concentrations. However, physical and bulk chemical conditions under which those experiments are conducted do not match well the conditions expected in a magma ocean. For all its faults, this study's very high temperature, depolymerized silicate melt, and natural silicate and S contents may be used to model partitioning behavior in a magma ocean environment.

For the purposes of the ensuing discussion, that applies these data to terrestrial Ag and Pd, we elect to use the lowest $D_{Pd}^{metallic\ sulfide/silicate}$ values obtained in this study. These values range from approximately 160–650 and are consistent with observed mantle depletions. The experiments that produced these values were conducted at 2 GPa, 2100–2400 °C, 7 wt% S in the metallic sulfide and a chondritic Fe/Si ratio. They also contained the lowest concentrations of Pd of any experiments in this study. The implications of these data are discussed in the next section.

Implications

A Core ^{107}Ag Signature in Mauna Loa Lavas?

Presently available data is inconclusive about the presence of elevated ^{107}Ag in Hawai'ian lavas. The limit of analytical precision is $\pm 1.3\varepsilon$ which is perilously close to observed signal of $+1.5\varepsilon$ relative to standard NIST SRM 978a. Furthermore, given the potential for low temperature processes to affect silver isotopic signatures, as may occur in silver ores, this slight signal does not prove core-mantle interaction. To better constrain the strength of the ^{107}Ag signal that would be expected from a core-polluted mantle plume, we combine Ag and Pd partitioning data from this study with a simple geochemical model. The model calculates the expected Ag isotopic composition for Mauna Loa lavas for various differentiation times, entrainment scenarios, and initial chemical conditions. Ideally, the model calculations will indicate whether a resolvable ^{107}Ag signature could exist in Hawai'ian lavas.

Table 3. Model parameters.

Model parameter	Value	Source
Lambda ^{107}Pd	1.06638×10^{-7} yr^{-1}	Parrington et al. (1996)
^{107}Pdi/total Pdi	6.35036×10^{-6}	Parrington et al. (1996)
^{107}Agi/total Agi	0.48161	Parrington et al. (1996)
^{107}Ag/^{109}Agi	1.07916	Carlson and Hauri (2001) (NIST SRM 978a)
Terrestrial Pd/Ag	20	McDonough (2003)
D_{Pd} metal/silicate	412	This study
D_{Ag} metal/silicate	28	This study
Fraction core material entrained	0.01	Brandon et al. (1998)

The parameters used to define the base case of this model are presented in Table 3. They were chosen to reasonably represent conditions that would have been present during a magma-ocean-based planetary differentiation and equilibration event. $D_{Ag}^{metallic\ sulfide/silicate}$ was calculated at 10% S, a reasonable S content for the core. $D_{Pd}^{metallic\ sulfide/silicate}$ was calculated using the average from the three low Pd experiments from this study. A terrestrial Pd/Ag of 20 was taken from McDonough (2003). Core material entrainment was estimated at 1% based loosely on the order of magnitude suggested by Brandon et al. (1998).

Figure 8 displays the expected ε^{107}Ag values for Mauna Loa lavas given the base case model parameters and three lengths of time before Earth's differentiation. Even with core formation occurring immediately after the conception of the solar nebula, resulting in maximum possible ^{107}Ag production, the calculated ε^{107}Ag is approximately 0.5, almost a factor of 3 smaller than observable by current analytical techniques (Carlson and Hauri 2001). While this value is low, there is considerable latitude permitted for choosing the model's input parameters. Changing the terrestrial Pd/Ag from the 20 of McDonough (2003) to the 88 of Carlson and Hauri (2001) would increase ε^{107}Ag to over 1.8, placing it in line with the observed signal, but requiring immediate core formation. Alternatively, with Pd/Ag of 20 but adjusting $D_{Ag}^{metallic\ sulfide/silicate}$ to the minimum permitted by the experimental error bars would increase ε^{107}Ag to approximately 1. In this case, slightly more entrainment of core material in the plume would raise the Ag signature to the level observed. Any number of reasonable parameter adjustments from D values, to terrestrial Pd/Ag, fraction of core material

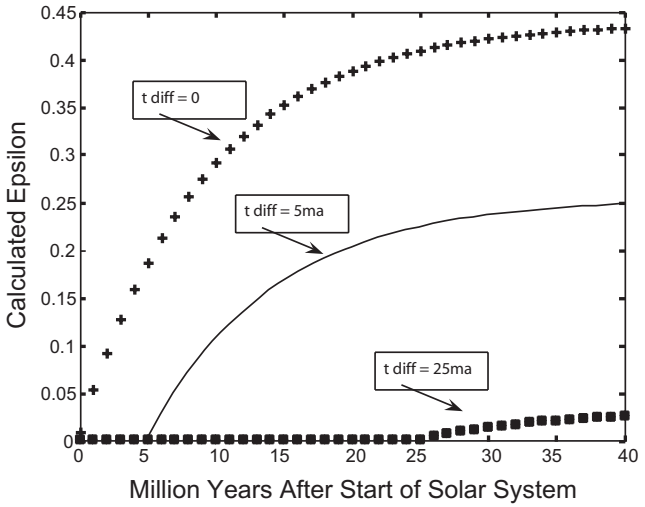

Fig. 8. Model calculations with the values provided in Table 3 for different times of planetary differentiation (t_{diff}). Even with immediate core formation ($t_{diff} = 0$), the expected Ag signature in the mantle plume would be below analytically resolvable levels (Carlson and Hauri 2001). There is considerable flexibility in the model parameters. Adjusting Pd/Ag from 20 of McDonough (2003) to 88 of Carlson and Hauri (2001) or using the lowest $D_{Ag}^{metallic\ sulfide/silicate}$ within error would more than triple the ^{107}Ag signal but still leave it at the threshold on analytic uncertainty.

entrained, and timing of core formation can be made to alter the model output to a range approximately equal to analytical uncertainty. However, producing a ^{107}Ag signature resolutely distinguishable above analytical uncertainty would require assumptions inconsistent with mainstream conceptions about Earth. We therefore conclude that if there is a core component present in Mauna Loa lavas, its manifestation in the ^{107}Ag signature would barely be distinguishable outside the bounds of analytical uncertainty.

Pd, Ag, and Observed Mantle Depletions

With the exception of Righter et al. (2006, 2008) and this study, experimentally and observationally derived mantle depletions for Pd have not agreed (Fig. 4). Ag, in contrast, is observed to be depleted in the mantle by a factor of 10–100, consistent with a one atmosphere experiment by Jones and Drake (1986) predicting a depletion of 3. Pd concentration observation yields calculated depletions of 10^{-2} to 10^{-3} in the mantle while experimental D commonly yields calculated depletions of 10^{-3} to 10^{-5} relative to bulk Earth.

$D_{Ag}^{metallic\ sulfide/silicate}$ measured in this study corresponds closely to observed depletions, supporting the conclusion drawn from the Jones and Drake (1986) datum that no severe experiment-observation inconsistency exists. While this study's high S content experiments resulted in very low $D_{Ag}^{metallic\ sulfide/silicate}$, the increase in $D_{Ag}^{metallic\ sulfide/silicate}$ with decreasing S content yields experimental values consistent with observation at S contents of less than 10 wt% in the metal. As the core is not likely to contain more than 10 wt% S, it is possible to conclude that our experimental data are reasonably consistent with observation (Fig. 4).

While the systematics of Pd partitioning in this system are not yet well understood, $D_{Pd}^{metallic\ sulfide/silicate}$ values for this study's most Pd-poor experiments overlap observed Pd mantle depletions. Three experiments from this study resulted in a $D_{Pd}^{metallic\ sulfide/silicate}$ that yields mantle depletions between 10^{-2} and 10^{-3}, on the same order of magnitude as the observed depletions. To the extent that the chemical and physical characteristics of this study's experiments permit authentic magma ocean metallic sulfide/silicate segregation, equilibration, and partitioning behavior, observed mantle Pd depletions are consistent with this experimental scenario, thereby eliminating the "siderophile element problem" for Pd and consequently the need for a "late veneer" to raise the mantle's Pd content (Fig. 4). Recently, Righter et al. (2006, 2008) reached the same conclusion with their experimental data. Furthermore, data offering resolution to the excess siderophile element problem have been present in the literature since the earliest Pd partitioning experiments. Fleet et al. (1991) $D_{Pd}^{metallic\ sulfide/silicate}$ values broadly decrease with decreasing metallic sulfide Pd contents (Fig. 6a). Extrapolation of this trend to plausible core Pd contents of 3 ppm (McDonough 2003) yield $D_{Pd}^{metallic\ sulfide/silicate}$s on the order of 600, the same value inferred by mantle observations, data from our study, and data from Righter et al. (2006, 2008). Although Pd mantle abundances require no late veneer, this may not be true for all HSE (cf. Brenan and McDonough 2009).

CONCLUSION

Even if Hawai'ian lavas contain core material, their plausible ^{107}Ag enrichment would not likely be resolvable within current analytical uncertainty. Thus, ^{107}Ag is presently unable to meaningfully address the issues of core-mantle interaction, timing of core formation and origin of mantle plumes.

Pd partitioning behavior in the liquid metal-liquid silicate system depends on total Pd content. Moreover, scrutiny of the new partitioning data at high experimental Pd contents reveal unexpectedly decreasing silicate Pd contents with increasing Pd in the charge as a whole. This behavior is consistent with curved silicate Pd saturation surfaces in the metallic sulfide–silicate Pd ternary. $D_{Pd}^{metallic\ sulfide/silicate}$ values for experiments with low Pd contents coincide well with mantle depletions suggesting that mantle Pd contents could have been set by liquid metallic sulfide-liquid silicate

equilibrium in a shallow magma ocean early in Earth's history. Similarly, experimentally derived $D_{Ag}^{metallic}_{sulfide/silicate}$ values from this study are consistent with observed mantle depletions, providing further support for planet-wide chemical equilibration in a magma ocean.

Acknowledgments—We thank Richard Ashe for guidance on the LA-ICP-MS and Charlie Mandeville for assistance on the electron microprobe. Additionally, comments from Steve Goldstein, Ed Mathez, John Longhi, and Peter Keleman greatly enhanced the quality and content of this work. We thank Richard Carlson, Nancy Chabot, Tim Jull, and 3 anonymous reviewers for their review wisdom and editorial assistance. This work was supported by the NSF and is LDEO contribution #7417.

Editorial Handling—Dr. A. J. Timothy Jull

REFERENCES

Bezmen N. I., Asif M., Brugmann G. E., Romanenko I. M., and Naldrett A. J. 1994. Distribution of Pd, Ru, Rh, Ir, Os, and Au between sulfide and silicate melts. *Geochimica et Cosmochimica Acta* 58:1251–1260.

Borisov A. and Palme H. 1996. Experimental determination of the solubility of Au in silicate melts. *Mineralogy and Petrology* 56:297–312.

Borisov A., Palme H., and Spettel B. 1994. Solubility of palladium in silicate melts: Implications for core formation in the earth. *Geochimica et Cosmochimica Acta* 58:705–716.

Brandon A., Walker R. J., Morgan J. W., Norman M. D., and Prichard H. M. 1998. Coupled ^{186}Os and ^{187}Os evidence for core-mantle interaction. *Science* 280:1570–1573.

Brenan J. M. and McDonough W. M. 2009. Core formation and metal-silicate fractionation of osmium and iridium from gold. *Nature Geoscience* doi:10.1038/ngeo658.

Capobianco C. J., Jones J. H., and Drake M. J. 1993. Metal-silicate thermochemistry at high-temperature—Magma oceans and the excess siderophile element problem of the earth's upper mantle. *Journal of Geophysical Research-Planets* 98:5433–5443.

Carlson R. W. and Hauri E. H. 2001. Extending the ^{107}Pd-^{107}Ag chronometer to low Pd/Ag meteorites with multicollector plasma-ionization mass spectrometry. *Geochimica et Cosmochimica Acta* 65:1839–1848.

Chabot N. L. and Drake M. J. 1997. An experimental study of silver and palladium partitioning between solid and liquid metal, with applications to iron meteorites. *Meteoritics & Planetary Science* 32:637–645.

Chen J. H. and Wasserburg G. L. 1996. Live ^{107}Pd in the early solar system and implications for planetary evolution. In *Earth processes: Reading the isotopic code*, AGU Monograph 95, edited by Basu A. and Hart S. Washington, DC.: AGU. pp. 1–20.

Cottrell E. A. and Walker D. 2006. Constraints on core formation from Pt partitioning in mafic silicate liquids at high temperatures. *Geochimica et Cosmochimica Acta* 70:1565–1580.

Crocket J. H., Fleet M. E., and Stone W. E. 1997. Implications of composition for experimental partitioning of platinum-group elements and gold between sulfide liquid and basaltic melt: The significance of nickel content. *Geochimica et Cosmochimica Acta* 61:4139–4149.

Dasgupta R. and Walker D. 2008. Carbon solubility and core melts in a shallow magma ocean environment and distribution of carbon between the Earth's core and mantle. *Geochimica et Cosmochimica Acta* 72:4627–4641.

Drake M. J. and Righter K. 2002. Determining the composition of the Earth. *Nature* 416:39–44.

Fleet M. E., Crocket J. H., and Stone W. E. 1991. Partitioning of palladium, iridium, and platinum between sulfide liquid and basalt melt: Effects of melt composition, concentration, and oxygen fugacity. *Geochimica et Cosmochimica Acta* 55:2545–2554.

Fleet M. E., Crocket J. H., and Stone W. E. 1996. Partitioning of platinum-group elements (Os, Ir, Ru, Pt, Pd) and gold between sulfide liquid and basalt melt. *Geochimica et Cosmochimica Acta* 60:2397–2412.

Fleet M. E., Crocket J. H., Liu M., and Stone W. E. 1999. Laboratory partitioning of platinum-group elements (PGE) and gold with application to magmatic sulfide-PGE deposits. *Lithos* 47:127–142.

Hauri E. H., Carlson R. W., and Bauer J. 2000. The timing of core formation and volatile depletion in solar system objects from high-precision ^{107}Pd-^{107}Ag isotope systematics (abstract #1812). 31st Lunar and Planetary Science Conference. CD-ROM.

Hillgren V. J., Drake M. J., and Rubie D. C. 1994. High-pressure and high-temperature experiments on core-mantle segregation in the accreting Earth. *Science* 264:1442–1445.

Hirose K. and Kushiro I. 1993. Partial melting of dry peridotites at high pressures: Determination of compositions of melts segregated from peridotite using aggregates of diamond. *Earth and Planetary Science Letters* 114:477–489.

Holzheid A., Sylvester P., O'Neill H. St. C., Rubie D. C., and Palme H. 2000. Evidence for a late chondritic veneer in the Earth's mantle from high-pressure partitioning of palladium and platinum. *Nature* 406:396–399.

Jana D. and Walker D. 1997. The influence of sulfur on partitioning of siderophile elements. *Geochimica et Cosmochimica Acta* 61:5255–5277.

Jana D. and Walker D. 1998. Core formation in the presence of various C-H-O volatile species. *Geochimica et Cosmochimica Acta* 63:2299–2310.

Jones J. H. and Drake M. J. 1986. Geochemical constraints on core formation in the Earth. *Nature* 332:221–228.

Jones J. H. and Malvin D. J. 1990. A nonmetal interaction model for the segregation of trace metals during solidification of Fe-Ni-S, Fe-Ni-P, and Fe-Ni-S-P alloys. *Metallurgical Transactions B* 21:697–706.

Kelly W. R. and Wasserburg G. J. 1978. Evidence for the existence of ^{107}Pd in the early solar system. *Geophysical Research Letters* 5:1079–1082.

Longerich H. P., Jackson S. E., and Günther D. 1996. Laser ablation inductively coupled plasma mass spectrometric transient signal data acquisition and analyte concentration calculation. *Journal of Analytical Atomic Spectrometry* 11:899–904.

McDonough W. F. 2003. Compositional model for the Earth's core. *The mantle and core*, edited by Carlson R. W. Treatise on Geochemistry, vol. 2. pp. 425–449.

McDonough W. F. and Sun S.-S. 1995. The composition of the Earth. *Chemical Geology* 120:223–253.

Newsom H. E. 1990. Accretion and core formation in the earth: Evidence from siderophile elements. In *Origin of the Earth*, edited by Newsom H. E. and Jones J. Oxford: Oxford University Press. pp. 273–288.

Newsom H. and Sims K. W. W. 1991. Core formation during early accretion of the Earth. *Science* 252:926–933.

Newsom H. E., Sims K. W. W., Noll P. D., Jaeger W. L., Maehr S. A., and Beserra T. B. 1996. The depletion of tungsten in the bulk silicate Earth: Constraints on core formation. *Geochimica et Cosmochimica Acta* 60:1155–1169.

O'Neill H. S., Dingwell D. B., Borisov A., Spettel B., and Palme H. 1995. Experimental petrochemisty of some highly siderophile elements at high temperatures, and some implications for core formation and the mantle's early history. *Chemical Geology* 120:255–273.

Palme H. and Jones J. 2003. Solar system abundances of the elements. *Meteorites, comets, and planets*, edited by Davis A. M. Treatise on Geochemistry vol. 1, pp. 41–61.

Parrington J. R., Knox H. D., Breneman S. L., Baum E. M., and Feiner F. 1996. *Nuclides and isotopes*, 15th ed. San Jose, CA: General Electric Nuclear Energy. 64 p.

Peach C. L., Mathez E. A., and Keays R. R. 1990. Sulfide melt-silicate melt distribution coefficients for noble metals and other chalcophile elements as deduced from MORB: Implications for partial melting. *Geochimica et Cosmochimica Acta* 54:3379–3399.

Peach C. L., Mathez E. A., Keays R. R., and Reeves S. J. 1994. Experimentally determined sulfide melt-silicate melt partition coefficients for iridium and palladium. *Chemical Geology* 117:361–377.

Ribe N. M. and Christensen U. R. 1999. The dynamical origin of Hawaiian volcanism. *Earth and Planetary Science Letters* 171:517–531.

Righter K. and Drake M. J. 1997. Metal/silicate equilibrium in a homogeneously accreting Earth: New results for Re. *Earth and Planetary Science Letters* 146:541–553.

Righter K. and Drake M. J. 1999. Effect of water on metal/silicate partitioning of siderophile elements: A high pressure and temperature terrestrial magma ocean and core formation. *Earth and Planetary Science Letters* 171:383–399.

Righter K. and Drake M. J. 2000. Metal/silicate equilibrium in the early Earth: New constraints from volatile moderately siderophile elements Ga, Sn, Cu and P. *Geochimica et Cosmochimica Acta* 64:3581–3597.

Righter K. and Drake M. J. 2003. Partition coefficients at high pressure and temperature. *The mantle and core*, edited by Carlson R. W. Treatise on Geochemistry, vol. 2. pp. 425–449.

Righter K., Humayun M., and Danielson L. 2006. Highly siderophile elements in the terrestrial upper mantle require a late veneer? New results for palladium (abstract #4040). Workshop on Early Planetary Differentiation 2006. Houston, Texas: Lunar and Planetary Institute.

Righter K., Humayun M., and Danielson L. 2008. Partitioning of palladium at high pressures and temperatures during core formation. *Nature Geoscience* 1, doi:10.1038/ngeo180.

Sattari P., Brenan J. M., Horn I., and McDonough W. F. 2002. Experimental constraints on the sulfide- and chromite-silicate melt partitioning behavior of rhenuim and platinum-group elements. *Economic Geology* 97:385–398.

Schonbachler M., Carlson R. W., Horan M. F., and Hauri E. H. 2007. The timescale of the Earth's accretion and volatile loss: New constraints from Pd-Ag systematics. Goldschmidt Conference Abstracts A904. Goldschmidt Conference 2007.

Schonbachler M., Carlson R. W., Horan M. F., Mock T. D., and Hauri E. H. 2008. Silver isotope variations in chondrites: Volatile depletion and the initial ^{107}Pd abundance of the solar system. *Geochimica et Cosmochimica Acta* 72:5330–5341.

Stone W. E., Crocket J. H., and Fleet M. E. 1990. Partitioning of palladium, iridium, platinum, and gold between sulfide liquid and basalt melt at 1200 °C. *Geochimica et Cosmochimica Acta* 54:2341–2344.

Van Keken P. E., Hauri E. H., and Ballentine C. J. 2002. Mixing in the mantle and the creation, preservation and destruction of mantle heterogeneity. *Annual Reviews in Earth and Planetary Science* 30:493–526.

Walker D. and Agee C. B. 1989. Partitioning "equilibrium," temperature gradients, and constraints on earth differentiation. *Earth and Planetary Science Letters* 96:49–60.

Walker D. and Li J. 2008. Molybdenum partitioning to 60 kilobars along a warped Fe-FeS liquidus. *Chemical Geology* 248:166–173.

Walker R. J., Morgan J. W., and Horan M. F. 1995. ^{187}Os enrichment in some mantle plume sources: Evidence for core-mantle interaction? *Science* 269:819–822.

Wheeler K. T. 2007. Experimental studies of U, Pd, Ag and Pb: Partitioning and phase stability. Ph.D. thesis, Columbia University, New York, NY, USA.

Wheeler K. T., Walker D., Fei Y., Minarik W. G., and McDonough W. F. 2006. Experimental partitioning of uranium between liquid iron sulfide and liquid silicate: Implications for radioactive heating in the Earth's core. *Geochimica et Cosmochimica Acta* 70:1537–1547.

Wood B. J. and Halliday A. N. 2010. The lead isotopic composition of the Earth can be explained by core formation alone. *Nature* 465, doi:10.1038/nature09072.